89-1187-CP

AEROELASTIC STABILITY AND CONTROL OF A HIGHLY FLEXIBLE AIRCRAFT

M.C. van Schoor †

S.H. Zerweckh ••

A.H. von Flotow *

Massachusetts Institute of Technology

Cambridge, Massachusetts

Abstract

This paper describes the aeroelastic analysis performed on a human-powered aircraft. The unique structural characteristics of this aircraft, namely; very flexible wings, high aspect ratio and low wing loadings, are typical of proposed high altitude long endurance aircraft. Because of these unique features, the aircraft exhibits uncommon aeroelastic characteristics. The structural dynamics of the airplane was obtained from a finite element model of the aircraft. In an assumed mode approach, a sub-set of the the natural mode shapes were used to calculate the quasi-steady and unsteady generalized modal forces using a two-dimensional strip model, which included unsteady drag and leading edge suction forces. The aeroelastic model predicted the airplane to be stable (at both sea level and high altitude), except for a mildly unstable phugoid mode. The results concluded that unsteady aerodynamics are significant for these type of aircraft and that the flexibility of the aircraft must be include to correctly model the dynamics for control purposes. A final conclusion was that the dynamics of the aircraft are very dependent on the flight conditions (speed and altitude).

Nomenclature

$C_{D_{Induced}}$	-	Induced drag
C_{D_o}	-	Parasite drag coefficient
$C^i_{L_\alpha}$	-	Slope of lift curve
C_{M_o}	-	Aerodynamic moment about the aerodynamic center
b	-	Half chord = c/2
d, D	-	Damping, damping matrix
e	-	Oswald's efficiency factor
m, M	-	Mass, mass matrix
k, K	-	Stiffness, stiffness matrix
q_∞	-	Free stream dynamic pressure = $\frac{1}{2}\rho U_\infty^2$
s	-	Width of the aerodynamic strip in the spanwise direction
U_∞	-	Free stream velocity
u, v, w	-	X-, Y- and Z- displacements/ deformations respectively
$\dot{u},\dot{v},\dot{w}$	-	Velocities in the X-, Y- and Z-directions respectively.

Greek:

ϕ, θ, ψ	-	Rotations about the X-, Y- and Z-axes respectively

Subscripts:

e	-	Equilibrium or steady state
d	-	Dynamic or perturbed
i	-	Index to identify aerodynamic strip
u	-	Unsteady

Introduction

The technology developed during MIT's Daedalus human-powered aircraft program has created the possibility of developing a high altitude, long endurance aircraft. These aircraft [Hall, et al] will need to be very light and aerodynamically efficient in order to stay aloft for long periods of time, using on board fuel, solar or micro-wave power. These aircraft will be characterized by high aspect ratio wings, low wing loadings, very flexible structures, reduced frequencies ($k = \omega b_r/U_\infty$) ranging from 0.06 to 0.6, and air apparent mass as high as 35% of the total aircraft mass. The general assumption that aircraft rigid and flexible body dynamics can be separated cannot be applied to these aircraft. Spectral separation of rigid body and structural dynamics is not justified, nor is the approximation of quasi-steady aerodynamics.

This paper describes the aeroelastic modeling and analysis of MIT's Michelob Light Eagle (MLE) human powered airplane (Fig. 1). The MLE extended the world distance record for Human Powered Aircraft to 58 km in January 1987 and served as a prototype for the Daedalus aircraft which extended the record to 130 km in the Spring of 1988. The high aspect ratio and the Reynolds number at nominal flight speed of the MLE is comparable to those expected of high altitude, long endurance aircraft.

† Graduate Student, Student Member AIAA

•• Graduate Student, Member DGLR

* Assistant Professor, Member AIAA

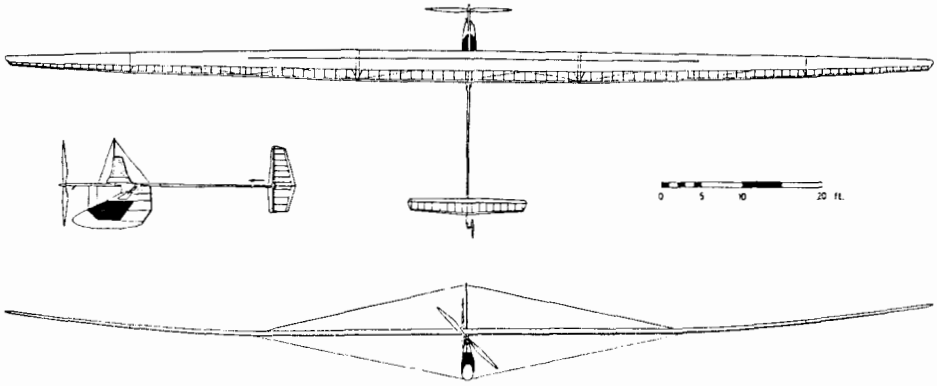

Figure 1 The Michelob Light Eagle Airplane.

One might thus view the research reported in this paper as being prototypical of that required for the development of such high altitude, long endurance aircraft. Table 1 summarizes the aerodynamic and structural properties of the MLE aircraft.

Zerweckh and von Flotow [Zerweckh, et al, 1988a and 1988b] outlined the attempted identification of the stability derivatives [Hill] of the MLE, from flight test data using a parameter identification program based upon assumed rigid body dynamics with quasi-steady aerodynamics. Using these stability derivatives, the frequency of both the short period and phugoid mode was predicted to be within the range of the in-flight observed structural frequencies. This result led to the conclusion that aeroelastic effects could not be ignored in modeling the stability and control characteristics of the MLE. The research reported in this paper thus includes the aeroelastic and unsteady aerodynamic effects in the stability model in order to not only improve the analytical stability and control predictions, but also to investigate the importance of these effects.

The structural dynamic model required for the aeroelastic analysis, was obtained by modeling the MLE primary structure with finite elements. Beam finite elements were used, where the beam properties were obtained from the original structural design. For the aerodynamic model the MLE's aerodynamic surfaces were divided into a finite number of two-dimensional strips. The aerodynamic lift and drag forces, as well as the aerodynamic moment, were calculated at the center of each of these aerodynamic strips. The aerodynamic forces (and moments) were a combination of the steady, quasi-steady and unsteady lift, drag and moments acting on the strip. The motion of the aircraft was expressed in terms of a linear combination of a small set of assumed modes. A good set of assumed modes was generated by modal analysis of the structural model mass loaded with the air apparent mass. The aerodynamic forces were integrated over the aircraft to yield the generalized aerodynamic forces. The generalized structural characteristics, namely; the modal mass, damping and stiffness matrices, were combined with these generalized modal aerodynamic forces, yielding an aeroelastic model from which the aeroelastic stability could be predicted as a function of flight speed and altitude.

The aeroelastic model was used to predict the stability of the aircraft for various levels of simplification. A model where only symmetric modes were retained was used to determine the relative importance of the flexible modes on the longitudinal stability of the aircraft. This was achieved by comparing the results of this model with the results of a model that contained only the three rigid body longitudinal modes. The flexible model was also used to quantify the effect of unsteady aerodynamics on the aeroelastic model and to predict the stability characteristics of the MLE at high altitude. Finally, given the slight asymmetry of the MLE, a model that incorporated all the rigid body modes as well as the first eight flexible modes was used to determine whether the exclusion of the lateral dynamics from the longitudinal model were justified.

Aeroelastic Model

An aeroelastic model requires both a structural dynamic model and an aerodynamic model of the MLE. The next sections describe how these models were obtained.

Structural Dynamic Model

The MLE design was based on a detailed structural analysis. For this research, the structural information used in the structural analysis was used to model the aircraft with a finite beam element model (See Fig. 2). For example; the wing was modelled with 8 finite beam elements. The beam properties, namely; EI, GJ, EA, mass and inertia were

Table 1: MLE Aerodynamic and Structural Properties

Aerodynamic Properties			
Wing Area (m^2)	32.8	Drag Area (m^2)	0.8
Wing Span (m)	34.7	Aspect Ratio	36.7
Empty Weight (kg)	42.0	Mass (With Pilot) (kg)	112.8
Design Power (W)	225.0	Design Airspeed (m/s)	7.0
Wing Loading (N/m^2)	34.0		
Moment of Inertia's:			
Without Apparent Mass		*With Apparent Mass*	
Ix (kgm^2)	2002	Ix (kgm^2)	3920
Iy (kgm^2)	205	Iy (kgm^2)	340
Iz (kgm^2)	2086	Iz (kgm^2)	2910

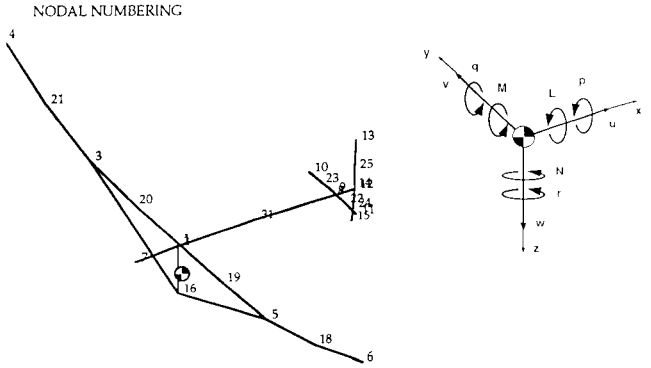

Figure 2 Finite element model of the MLE with nodal numbering and axis system.

obtained by using the average of these properties over the element length. The mass of the ribs and the air contained inside the wing were split and lumped at the two beam nodes. The air contained inside the wing is roughly 16% of the total wing mass. The only modification to the finite element model was to adjust the EI values, so that the static deflections predicted by the finite element model matched the in-flight observed deflections of the wing at the lift-wire attachment points and at the wing tips. This was achieved by loading the finite element model of the aircraft with the steady aerodynamic loads and comparing the analytical deflections with the in-flight observed deflections. The modified EI values were within 15% of the original values. No further experimental results exist with which the structural dynamic model could be verified or improved. Thus the validity of the results obtained is unverified and the work must be considered a pre-liminary study.

The finite element program ADINA was used to determine the structural dynamic characteristics of

Table 2: Summary of Structural Dynamic Characteristics (With Sea Level Apparent Mass)

Mode Number	Frequency (Hz)	Description
1	0.0	Rigid body X-translation
2	0.0	Rigid body Y-translation
3	0.0	Rigid body Z-translation
4	0.0	Rigid body rotation about X-axis
5	0.0	Rigid body rotation about Y-axis
6	0.0	Rigid body rotation about Z-axis
7	0.559	1st Symmetric wing bending
8	0.677	Tailboom rotation
9	0.879	1st Asymmetric wing bending
10	1.134	1st Symmetric wing bending (fore-aft)
11	1.183	1st Tailboom bending (X-Y plane)
12	2.267	1st Tailboom bending (X-Z plane)
13	2.336	2nd Symmetric wing bending
14	2.603	2nd Asymmetric wing bending
15	2.919	1st Wing Asymmetric Torsion
16	4.147	3rd Wing Symmetric Bending

the MLE and the results are depicted in Fig. 3 and summarized in Table 2. These figures were generated by adding auxiliary nodes to the beam finite element model to define the deflections of the aerodynamic surfaces and to graphically display the motion. The deflection at the auxiliary nodes was obtained by combining the nodal deflection and rotation of the beam generating node. The program that calculated the unsteady aerodynamic modal forces required the modal deflections and rotations at the half chord point of the selected aerodynamic strips. With the mode shapes defined as surfaces, these deflections and rotations could be calculated by fitting two-dimensional splines to the mode shapes.

The model with which the results of Fig. 3 were obtained included the apparent air mass. At sea level the apparent mass is approximately 35% of the total airplane mass and was added to obtain the best possible set of assumed modes for the unsteady

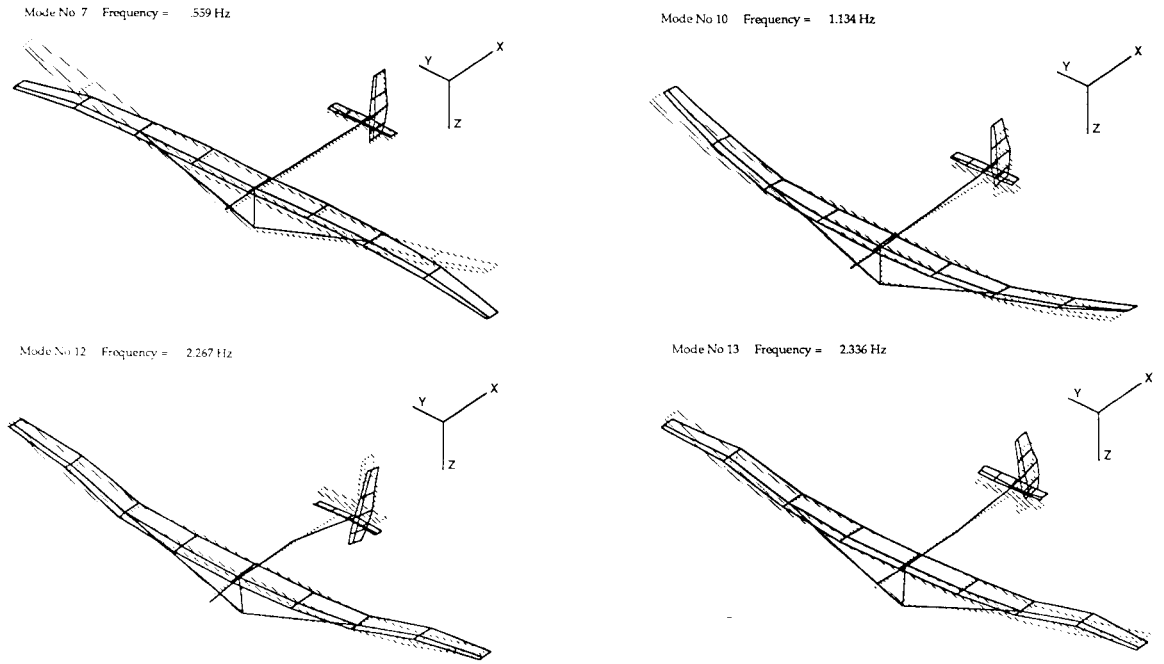

Figure 3 The first four flexible symmetric mode shapes of the MLE with apparent mass (sea level air density).

aerodynamic model. However, since the apparent mass was also included in the aerodynamic forces, the apparent mass was removed from the generalized structural mass matrix, yielding a non-diagonal modal mass matrix.

Pure rigid body modes, translation or rotation about one of the structural reference axes, were generated to enable the separation of longitudinal and lateral dynamics. The rigid body mode shapes generated by ADINA, as is typical of finite element programs, were linear combinations of the these motions.

Unsteady Aerodynamic Model

The unsteady aerodynamic forces could have been obtained using a standard kernel function [Cunningham] or doublet lattice program. This approach was not taken for several reasons. A unique feature of the MLE structure is the very low stiffness of the main wing in the fore-aft direction. The first wing fore-aft symmetric bending mode falls between the first and second vertical wing bending modes. Add to this the fact that the MLE's angle of attack at nominal flight speed is as high as 10 degrees, it was felt that unsteady drag terms should be included in the aerodynamic model [Boyd, Petre]. Thus, to consistently and correctly include all terms, the unsteady aerodynamics were calculated using a two-dimensional strip model of the MLE (See Fig. 4). Another reason which justifies the use of strip theory is that the power of panel methods is not needed for high aspect ratio aircraft.

The assumptions used in this model were that wing thickness effects could be ignored, the flow is incompressible and that the wing section has negligible chordwise deformations (it only pitches and plunges). The effect of one aerodynamic surface on another (for example: the wing on the elevator) was also ignored. Given the relatively small size, compared to the wing, of the other aerodynamic surfaces, this simplification seems justifiable. The model divided the aerodynamic surfaces, the main wing, elevator, rudder and cockpit into a finite number of aerodynamic strips. Given the size of the cockpit compared to the rudder, the cockpit was included in the aerodynamic model to correctly model the lateral dynamics. The contributions of the lift, drag and moment forces on a surface (i) can be transformed to yield the forces acting on the strip in the inertial reference frame (See Fig. 4 and 5). (Note the following equations are valid for the main wing and elevator but can easily be extended to be valid for the rudder and cockpit).

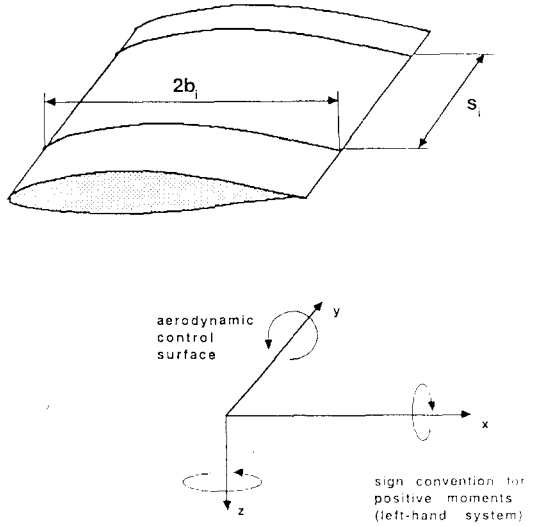

Figure 4 Two dimensional aerodynamic strip model with aerodynamic surface and sign convention.

The force in the x-direction:

$$F_i^x = -L_i^a \sin\theta_i + D_i \cos\gamma_i - F_i^s \cos\theta_i \qquad (1)$$

The force in the z-direction:

$$F_i^z = -L_i^a \cos\theta_i - D_i \sin\gamma_i + F_i^s \sin\theta_i + W_i \qquad (2)$$

The pitching moment (y-axis) about the half chord point:

$$M_i^y = M_{i_o}^y - \frac{b_i}{2} L_i^a \qquad (3)$$

F_i^s is the unsteady leading edge suction force which arises from the inverse square root singularity of the vorticity distribution along the airfoil at its leading edge. The propulsive force can be seen to correct for the free-stream component of the lift which is computed normal to the airfoil, to yield a lift vector normal to the free-stream [Boyd, Greenberg, Garrick]. Considering small perturbations about straight and level flight, the following small angle approximations can be made to linearize the equations of motion:

$$\gamma_i = \gamma_i^e (=0) + \frac{\dot{w}_i}{U_\infty} = \frac{\dot{w}_i}{U_\infty} \qquad (4)$$

$$\theta_i = \theta_i^d + \theta_i^e = \theta_i + \theta_i^e \qquad (5)$$

The streamwise velocity at the half chord of the section is perturbed as:

$$U_i = U_\infty - \dot{u}_i \qquad (6)$$

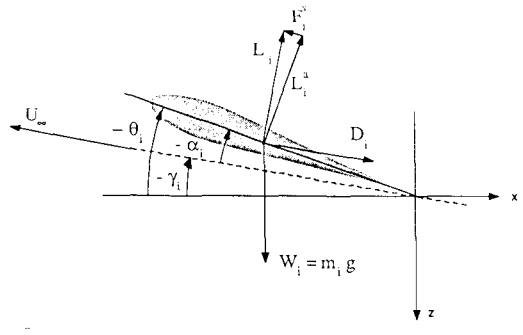

Figure 5 Forces acting on an aerodynamic strip with angle definition for the aerodynamic model.

Using these approximations, eq.'s 1 to 3, for small angles, become:

$$F_i^x = -L_i^a(\theta_i^e + \theta_i) + D_i - F_i^s \tag{1a}$$

$$F_i^z = -L_i^a - D_i\frac{\dot{w}_i}{U_\infty} + F_i^s(\theta_i^e + \theta_i) + W_i \tag{2a}$$

$$M_i^y = M_{i_o}^y - \frac{b_i}{2}L_i^a \tag{3a}$$

The total lift is a combination of the steady lift and the dynamic lift. The dynamic lift term is obtained from Dowell [Dowell, et al] and total lift is given by:

$$\begin{aligned} L_i^a = &-\rho(U_\infty - \dot{u}_i)^2 s_i b_i C_{L_\alpha}^i \theta_i^e \\ &+ \pi\rho s_i b_i^2[\ddot{w}_i - (U_\infty - \dot{u}_i)\dot{\theta}_i] \\ &+ C_{L_\alpha}^i \rho(U_\infty - \dot{u}_i) s_i b_i C(k_i)\Big[\dot{w}_i - \\ &- (U_\infty - \dot{u}_i)\theta_i - \frac{1}{2}b_i\dot{\theta}_i\Big] \end{aligned} \tag{7}$$

where $C(k_i)$ is the well known Theodorsen function [Bisplinghoff, et al]. In this research, unlike common practice, the reduced frequency was considered to be complex. The generalized Theodorsen's function is expressible in terms of modified Bessel functions of complex argument as [Edwards, Luke]:

$$C(k_r) = \frac{K_1(k_r)}{K_0(k_r) + K_1(k_r)} \tag{8}$$

The drag on the aerodynamic strip is:

$$D_i = \rho(U_\infty - \dot{u}_i)^2 s_i b_i\left(C_{D_o} + C_{D_{induced}}^i\right) \tag{9}$$

and the leading edge suction force is obtained from Boyd as:

$$\begin{aligned} F_i^s = &\, 2C_{L_\alpha}^i \rho(U_\infty - \dot{u}_i) s_i b_i\Big[-C(k_i)\,\dot{w}_i - \\ &+ (U_\infty - \dot{u}_i)C(k_i)\,\theta_i + \left(\frac{1}{2}C(k_i) - \frac{1}{2}\right)b_i\dot{\theta}_i\Big]\theta_i^e \end{aligned} \tag{10}$$

Two three dimensional effects are included in these expressions. The first was to assume that the lift is elliptically distributed along the aerodynamic surfaces. The section lift curve slope was given by the following expression:

$$C_{L_\alpha}^i = 2\pi C_o\sqrt{1 - \left(\frac{y_i}{y_{tip}}\right)^2} \tag{11}$$

where C_O is constant for a given aerodynamic surface (wing, elevator, etc) and determined to yield the correct steady total lift. The second three dimensional effect included was the induced drag term. The section induced drag [McCormick] was calculated as:

$$\frac{C_{L_\alpha}^{i\,2}\left(-\theta_i^e - \theta_i + \frac{\dot{w}_i}{U_\infty}\right)^2}{\pi e A} \tag{12}$$

Although this term is zero for wings of infinite span, the high steady state angle of attack, of 10 degrees, at nominal flight speed makes this term as important as the parasitic drag term. The moment about the center of the aerodynamic strip (mid-chord) is given by Dowell [Dowell, et al] as:

$$\begin{aligned} M_i^y = &\,\rho(U_\infty - \dot{u}_i)^2 s_i b_i^2 C_{M_o}^i \\ &+ \frac{1}{2}\rho(U_\infty - \dot{u}_i)^2 s_i b_i^2 C_{L_\alpha}^i \theta_i^e \\ &+ \pi\rho s_i b_i^2\begin{bmatrix} -\frac{1}{2}(U_\infty - \dot{u}_i)b_i\dot{\theta}_i \\ -\frac{1}{8}b_i^2\ddot{\theta}_i \end{bmatrix} \\ &+ \frac{C_{L_\alpha}^i}{2}\rho(U_\infty - \dot{u}_i) s_i b_i^2 C(k_i)\left[-\dot{w}_i\right. \\ &\left. + (U_\infty - \dot{u}_i)\theta_i + \frac{1}{2}b_i\dot{\theta}_i\right] \end{aligned} \tag{13}$$

Linearizing about the steady state (level flight), where the steady forces are in balance, the perturbational force (or moment) due to perturbations q_i is given by (also known as the Jacobian):

$$\delta F_j = \frac{\partial F_j}{\partial q_1}q_1 + \frac{\partial F_j}{\partial q_2}q_2 + \frac{\partial F_j}{\partial q_3}q_3 + \ldots \tag{14}$$

The governing differential equations were obtained by evaluating the partial derivatives of eq. 14. Setting all second order terms to zero and assuming a solution of the form:

$$\begin{aligned} u(x,y,z,t) &= u(x,y,z)e^{\lambda t} \\ w(x,y,z,t) &= w(x,y,z)e^{\lambda t} \\ \theta(x,y,z,t) &= \theta(x,y,z)e^{\lambda t} = \frac{dw(x,y,z)e^{\lambda t}}{dx} \end{aligned} \tag{15}$$

with:

$$k_i = \frac{k_r b_i}{b_r},\ \lambda = j\frac{k_r U_\infty}{b_r} \text{ and } \lambda^2 = -\left(\frac{k_r U_\infty}{b_r}\right)^2 \tag{16}$$

the aerodynamic perturbational forces and moment acting on the aerodynamic strip are given by:

$$\begin{aligned} \frac{\delta F_i^x}{q_\infty e^{\lambda t}} = &-\left[4s_i b_i C_{D_o}\right]\left(\frac{\lambda}{U_\infty}\right)u_i \\ &-\left[4s_i b_i \frac{C_{L_\alpha}^{i\,2}}{\pi e A}\right]\theta_i^e\left(\frac{\lambda}{U_\infty}\right)w_i \\ &+\left[2s_i b_i C_{L_\alpha}^i\right]\left(\frac{\lambda}{U_\infty}\right)\theta_i^e w_i \\ &-\left[2\pi s_i b_i^2\right]\theta_i^e\left(\frac{\lambda}{U_\infty}\right)^2 w_i \end{aligned}$$

$$+\left[4s_i b_i \frac{C^i_{L_\alpha}{}^2}{\pi e A}\right]\theta^e_i \theta_i$$
$$+\left(\frac{jk_r}{b_r}\right)\left[2s_i b_i (C(k_i)-1) C^i_{L_{\alpha_i}}\right]\theta^e_i w_i$$
$$+\left[2\pi s_i b_i^2 + s_i b_i^2 C^i_{L_\alpha}\right]\left(\frac{\lambda}{U_\infty}\right)\theta^e_i \theta_i$$
$$-\left[2s_i b_i (C(k_i)-1) C^i_{L_\alpha}\right]\theta^e_i \theta_i$$
$$-\left(\frac{jk_r}{b_r}\right)\left[s_i b_i^2 (C(k_i)-1) C^i_{L_{\alpha_i}}\right]\theta^e_i \theta_i \quad (17)$$

$$\frac{\delta F^z_i}{q_\infty e^{\lambda t}} = -\left[4s_i b_i C^i_{L_\alpha}\right]\left(\frac{\lambda}{U_\infty}\right)\theta^e_i u_i$$
$$-\left[2s_i b_i C^i_{L_\alpha} + 2s_i b_i C_{D_o}\right]\left(\frac{\lambda}{U_\infty}\right) w_i$$
$$-\left[2s_i b_i^2 \pi\right]\left(\frac{\lambda}{U_\infty}\right)^2 w_i$$
$$+\left[2s_i b_i C^i_{L_\alpha}\right]\theta_i$$
$$+\left[2s_i b_i^2 \pi + s_i b_i^2 C^i_{L_\alpha}\right]\left(\frac{\lambda}{U_\infty}\right)\theta_i$$
$$-\left(\frac{jk_r}{b_r}\right)\left[2s_i b_i (C(k_i)-1) C^i_{L_\alpha}\right] w_i$$
$$+\left[2s_i b_i (C(k_i)-1) C^i_{L_\alpha}\right]\theta_i$$
$$+\left(\frac{jk_r}{b_r}\right)\left[s_i b_i^2 (C(k_i)-1) C^i_{L_\alpha}\right]\theta_i \quad (18)$$

$$\frac{\delta M^y_i}{q_\infty e^{\lambda t}} = -\left[4s_i b_i^2 C^i_{M_o}\right]\left(\frac{\lambda}{U_\infty}\right) u_i$$
$$-\left[2s_i b_i^2 C^i_{L_\alpha}\right]\left(\frac{\lambda}{U_\infty}\right)\theta^e_i u_i$$
$$-\left[s_i b_i^2 C^i_{L_\alpha}\right]\left(\frac{\lambda}{U_\infty}\right) w_i$$
$$+\left[s_i b_i^2 C^i_{L_\alpha}\right]\theta_i$$
$$-\left[s_i b_i^3 \pi - \frac{1}{2} s_i b_i^3 C^i_{L_\alpha}\right]\left(\frac{\lambda}{U_\infty}\right)\theta_i$$
$$-\left[\frac{1}{4} s_i b_i^4 \pi\right]\left(\frac{\lambda}{U_\infty}\right)^2 \theta_i$$
$$-\left(\frac{jk_r}{b_r}\right)\left[s_i b_i^2 (C(k_i)-1) C^i_{L_\alpha}\right] w_i$$
$$+\left[s_i b_i^2 (C(k_i)-1) C^i_{L_\alpha}\right]\theta_i$$
$$+\left(\frac{jk_r}{b_r}\right)\left[\frac{1}{2} s_i b_i^3 (C(k_i)-1) C^i_{L_\alpha}\right]\theta_i \quad (19)$$

In these equations (b_r) is a reference length taken to be the half-chord length at the 70% span position. Note that for the vertical surfaces, namely the rudder and the cockpit, the deflections are in the y-direction (v) and the above equations can be extended to be valid for these surfaces by replacing (w) with (v) and (θ) with (ψ). Note that in these equations, terms containing (θ_e) are dependent on the equilibrium angle of attack and thus on flight speed. The terms containing (λ) were introduced in the equations of motion as mass, damping or stiffness terms. The {C(k) - 1} terms were calculated for a range of reference complex reduced frequencies $k_r = \rho_r e^{i\theta_r}$. The range of magnitude and phase angles of the reference reduced frequency was selected to cover the range of reduced frequencies expected in the stability analysis. Setting these terms equal to zero in the stability analysis program results in a quasi-steady aerodynamic model.

In an assumed mode approach, the deflections are assumed to be of the form:

$$u(x_i,y_i,z_i,t) = \sum_{n=1}^{m} \phi^x_n(x_i,y_i,z_i) e^{\lambda_n t}$$
$$v(x_i,y_i,z_i,t) = \sum_{n=1}^{m} \phi^y_n(x_i,y_i,z_i) e^{\lambda_n t}$$
$$w(x_i,y_i,z_i,t) = \sum_{n=1}^{m} \phi^z_n(x_i,y_i,z_i) e^{\lambda_n t} \quad (20)$$

with the slopes given by:

$$\psi(x_i,y_i,z_i,t) = \sum_{n=1}^{m} \frac{d\phi^y_n(x_i,y_i,z_i)}{dx} e^{\lambda_n t}$$
$$\theta(x_i,y_i,z_i,t) = \sum_{n=1}^{m} \frac{d\phi^z_n(x_i,y_i,z_i)}{dx} e^{\lambda_n t} \quad (21)$$

Using these expressions, the vector of generalized aerodynamic forces is given by:

$$Q = \phi^{x^T}\delta F^x + \phi^{y^T}\delta F^y + \frac{d\phi^{y}}{dx}^T \delta M^x +$$
$$\phi^{z^T}\delta F^z + \frac{d\phi^{z}}{dx}^T \delta M^y \quad (22)$$

where vectors F and M are given by eq.'s 17 to 19. In eq. 22 the aerodynamic forces, by the multiplication of the mode shape vectors (and their slopes), are integrated over the aircraft.

Aeroelastic Model

The MLE was divided into four structural surfaces, namely; wing, elevator, rudder and cockpit, and for each surface a separate two-dimensional spline was fitted to the mode shapes obtained from the structural dynamic model. The airplane was also divided into several aerodynamic strips and the deflection and rotation of the strip midchord point, required to calculate the aerodynamic loads on the strip (eq.'s 17 to 19), could be evaluated using these fitted splines. The generalized aerodynamic force matrix was obtained from eq. 22 and stored in the

following form:

$$Q = q_\infty \left[\left(Q^q_m \left(\frac{\lambda}{U_\infty} \right)^2 + Q^q_d \left(\frac{\lambda}{U_\infty} \right) + Q^q_s \right) + \left(Q^e_m \left(\frac{\lambda}{U_\infty} \right)^2 + Q^e_d \left(\frac{\lambda}{U_\infty} \right) + Q^e_k \right) \theta_e + Q_u \left(k = \frac{-j\lambda U_\infty}{b_r} \right) + Q^e_u \left(k = \frac{-j\lambda U_\infty}{b_r} \right) \theta_e \right] e^{\lambda t} \quad (23)$$

The complete aeroelastic description of the aircraft is:

$$\left[M(\rho)\lambda^2 + D(\rho, U_\infty, \theta_e)\lambda + K(\rho, U_\infty, \theta_e) - Q_{ua}(\rho, U_\infty, \theta_e, \lambda) \right] e^{\lambda t} = 0 \quad (24)$$

where **M**, **D**, and **K** contain contributions from the quasi-steady aerodynamic, while the unsteady modifications are lumped in Q_{ua}. Mass proportional damping and 2% structural damping ratios was assumed for the flexible modes.

Stability Analysis

In the stability analysis program the steady state angle of attack (θ_e) was calculated for each flight speed and altitude (air density). It was assumed that this angle is constant for a given aerodynamic surface (wing, elevator, etc). Given the steady state angle of attack, the corresponding terms in the generalized force matrices (eq. 24) were evaluated.

The aeroelastic stability characteristics were obtained by finding the eigenvalues of the characteristic equation. This was achieved using Mueller's method [Press, et al]; solving for the eigenvalues by finding the complex roots of the determinant of the characteristic equation (eq. 24). Mueller's method is an iterative Newton-Raphson scheme that converges rapidly on the roots given a good initial guess. At any given iteration, the reduced frequency (eq. 16) associated with the estimated root was calculated and the corresponding unsteady generalized force matrix was obtained by linear two-dimensional interpolation in the reduced frequency magnitude and phase plane. The error introduced by the interpolation for the generalized force matrix was minimized by careful selection of the range of reduced frequency magnitude and phase values for which these matrices were calculated. The convergence in finding the roots was significantly slowed by adding the unsteady aerodynamic terms.

The results of the aeroelastic stability analysis are presented in the form of root locii, where the solution at each flight speed is plotted on the real/imaginary plane. A root locus is only valid for the given altitude (air density) and, where deemed necessary, the results are also presented as frequencies or damping ratios versus air speed plots An important feature of the root finder program, is that in certain cases the program failed to find all the eigenvalues, especially if the eigenvalues changed from oscillatory to critically damped modes. In most cases the location of the missing root(s) can be inferred by inspection from the requirement that the root locus plot must be symmetric with respect to the real axis.

Results

Given the aeroelastic model, several key questions could be investigated. Not only could the aeroelastic stability characteristics be determined for control and performance purposes but also the relative importance of certain modeling terms. The very flexible structure of the MLE and the significant apparent mass fraction indicates that a control model can only be obtained from an aeroelastic analysis. The aeroelastic analysis would indicate the dependence of the control model on airspeed and altitude as well as which modes could be excluded from the model. On the other hand the aeroelastic model will also enable a structural engineer to reliably predict the fatigue characteristics of the aircraft and to identify or re-design critical structural components.

In identifying the relative importance of the modeling terms added to the aeroelastic model, the following questions were addressed. Are the unsteady aerodynamic terms important? Is it necessary to add the drag terms? Given no clear spectral separation between structural modes, how many flexible modes must be included in the aeroelastic model? These questions are addressed separately in the following paragraphs.

Control and Performance Issues

In order to determine the dependence of the eigenvalues on air speed and altitude, a nominal longitudinal model was analyzed. The nominal longitudinal model included the three longitudinal rigid body modes and the first five symmetric flexible modes (Modes 7, 10, 12, 13 and 16 - See Table 2). The root locii of Fig. 6 were obtained by increasing the airspeed from just below the stall speed of 6 m/s to 22 m/s with speed increments of 0.25 m/s. Fig. 6 is valid for flight at sea level and Fig. 9 for flight at an altitude of 20 km above sea level, with the arrows indicating the direction of increasing flight speed. In Fig. 9 the airspeed was varied from 20 m/s to 60 m/s in increments 0.25 m/s. In Fig. 7, the eigen-frequencies associated with the root locii of Fig. 6 are plotted versus airspeed and in Fig. 8 the damping ratios versus air speed. The aeroelastic model used is the complete unsteady aerodynamic model. From these figures the phugoid mode is predicted to have a frequency of 0.17 Hz and a damping ratio of 16% (of critical) at the nominal flight speed (7 m/s). The short period mode is critically damped with the frequency associated with the real root approximately 2.5 Hz. These values agree favorably with predictions obtained from a rigid body model [Etkin] using coefficients obtained from the parameter

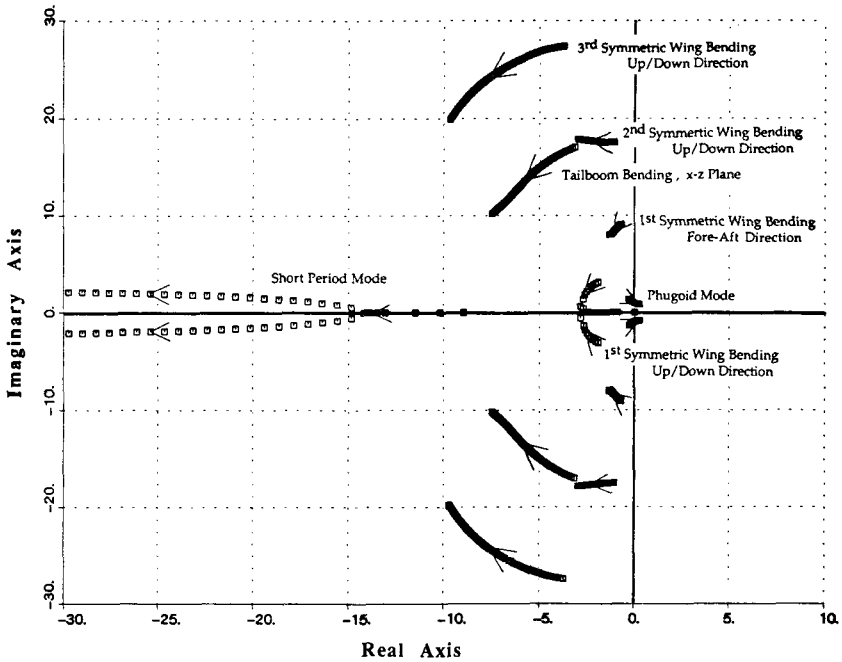

Figure 6 Root locus of the MLE flying at sea level (6-22 m/s). The root locus was obtained with the unsteady aerodynamic model and 8 symmetric assumed modes.

identification done by Zerweckh [Zerweckh, et al, 1988a].

Important to notice is the significant movement of all the eigenvalues with changing flight speed and the difference between the solutions at sea level and high altitude. At high altitudes, the air apparent mass approaches zero and the modal frequencies are closer to the in-vacuo frequencies. This change in modal separation alters the aeroelastic modal coupling and the overall conclusion is that any autopilot design will require static pressure dependent feedback gains and that aeroelastic effects cannot be ignored in the control design. The phugoid mode that becomes unstable at low altitudes, is a low frequency, very lightly (un)damped mode which should be easy to control. This mode is unstable for all flight speeds at high altitude. At low altitudes the first wing bending mode changes from an oscillatory mode to a critically damped mode as the flight speed increases. This response was verified by in-flight tests with the MLE. Another peculiar result at low altitudes is that the short period mode changes from a critically damped mode to an oscillatory mode as the flight speed increases. However, given the high damping ratio associated with the oscillatory behavior, this mode is in essence a critically damped mode.

From a structural engineering viewpoint the significant changes in frequencies and damping ratios indicates that the aeroelastic model is a pre-requisite for a reliable fatigue prediction.

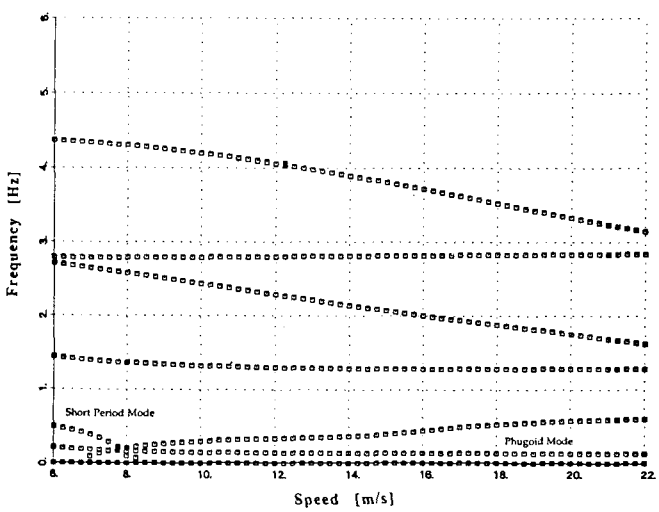

Figure 7 Predicted modal frequencies versus air speed of the 8 degree-of-freedom longitudinal model flying at sea level. Also see Figure 6.

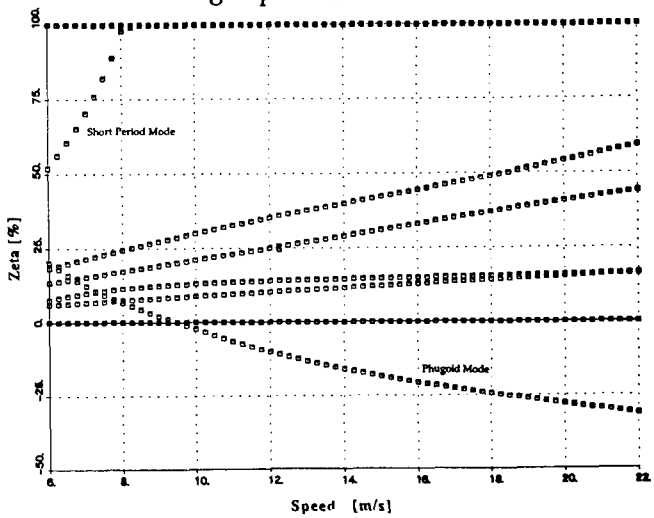

Figure 8 Predicted modal damping ratios versus air speed of the 8 degree-of-freedom longitudinal model flying at sea level. Also see Figure 6.

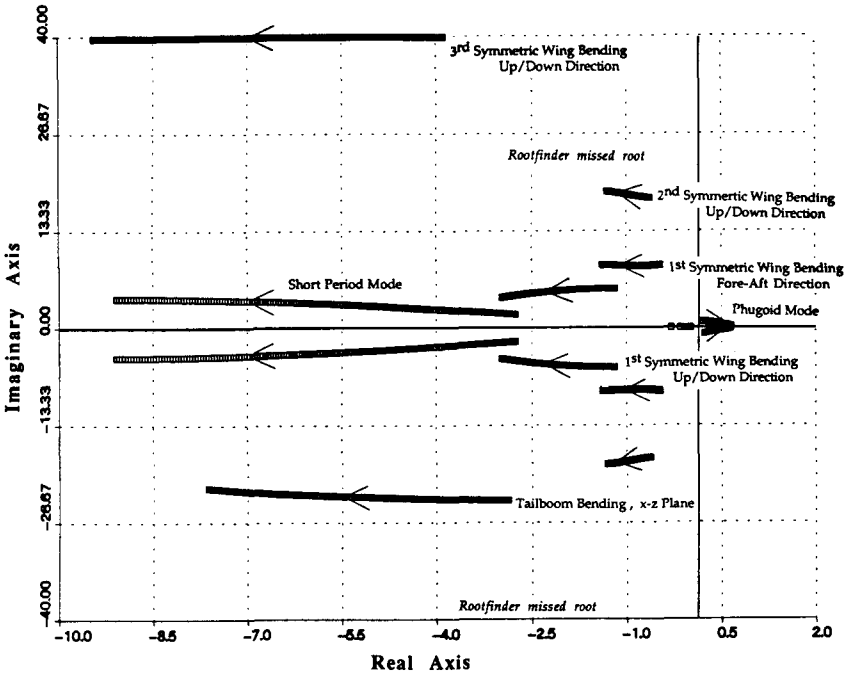

Figure 9 Root locus of the MLE flying at 20 km (20-60 m/s). The root locus was obtained with the unsteady aerodynamic model and 8 symmetric assumed modes.

Model Complexity Issues

Quasi-steady versus Unsteady Aerodynamics: In order to determine the relative importance of the unsteady aerodynamic terms, the aeroelastic analysis of Fig. 10 was repeated with a quasi-steady aerodynamic model (compare with Fig. 6). By comparing these two figures one can conclude that unsteady aerodynamic terms are significant and should be retained in the aeroelastic stability analysis.

Unsteady Aerodynamic Drag Terms: The general conclusion is that unsteady drag terms do not result in significant modal coupling between vertical bending and fore-aft bending modes. However, the unsteady drag terms do result in increased damping of the fore-aft bending modes (See Fig. 6) and retention of these terms may be required for reliable fatigue modeling.

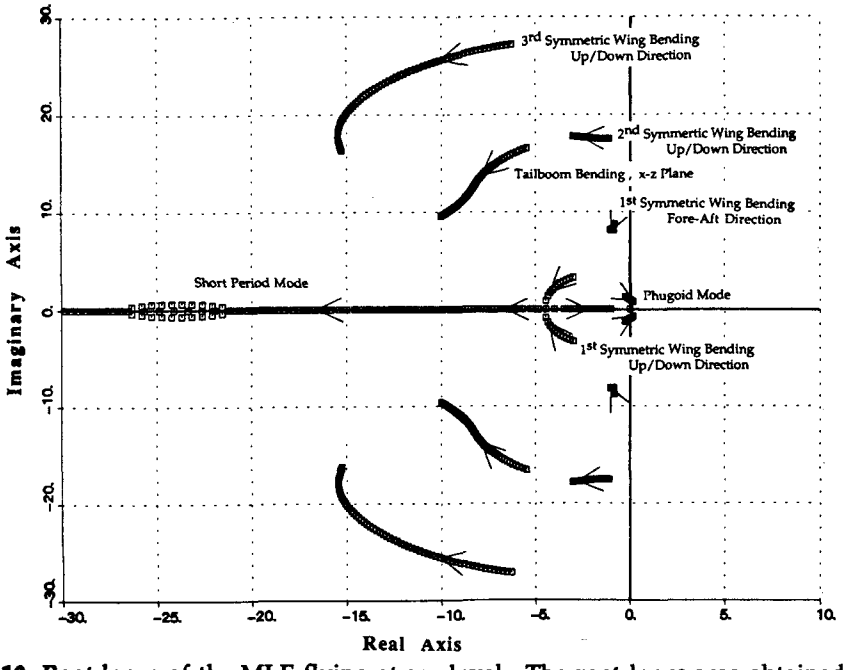

Figure 10 Root locus of the MLE flying at sea level. The root locus was obtained with a quasi-steady aerodynamic model and 8 symmetric assumed modes.

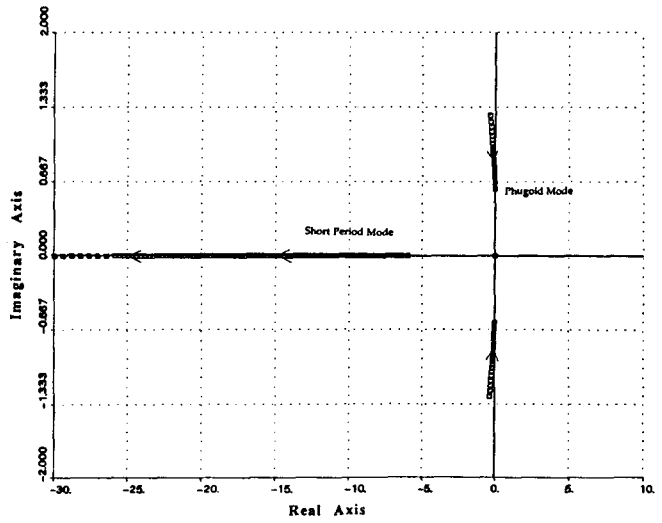

Figure 11 Root locus of the MLE flying at sea level (6-22 m/s). The root locus was obtained with the unsteady aerodynamic model and 3 symmetric (rigid body) assumed modes.

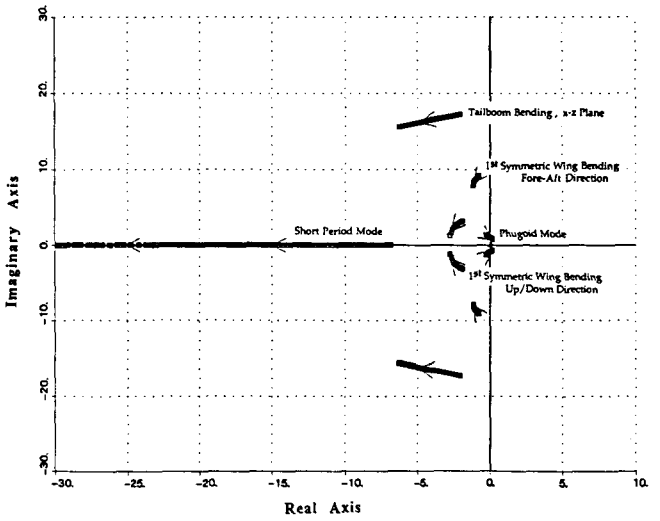

Figure 12 Root locus of the MLE flying at sea level (6-22 m/s). The root locus was obtained with the unsteady aerodynamic model and 6 (3 rigid body and 3 flexible) symmetric assumed modes.

Model Truncation: The effects of modal truncation are studied by studying the convergence of the stability results as the number of flexible modes are increased. Fig. 11 depicts the stability results for a three degree of freedom rigid body longitudinal model and Fig. 12 depicts the results for a longitudinal model that included the three rigid body modes and the first three symmetric flexible modes (Modes 7, 10, 12 - See Table 2). The analyses for these two figures were performed at sea level, using the complete unsteady aeroelastic model. Comparing these figures with Fig. 6, one can conclude that the stability results are significantly affected by the addition of the flexible modes. The rigid body model predicts a stable phugoid mode where the combined rigid and flexible model predicts a phugoid mode that goes unstable as the airspeed increases. The coarse discretization of the finite element model prevented the addition of more flexible modes to the rigid/flexible models to clearly identify the convergence of the results as the flexible mode number increases. The coarse mesh of the finite element model would yield incorrect higher frequency modes. Comparing Fig. 6 to Fig. 12 one can conclude that the addition of the two extra flexible modes did not alter the lower frequency mode's behavior, only the behavior of the higher frequency modes.

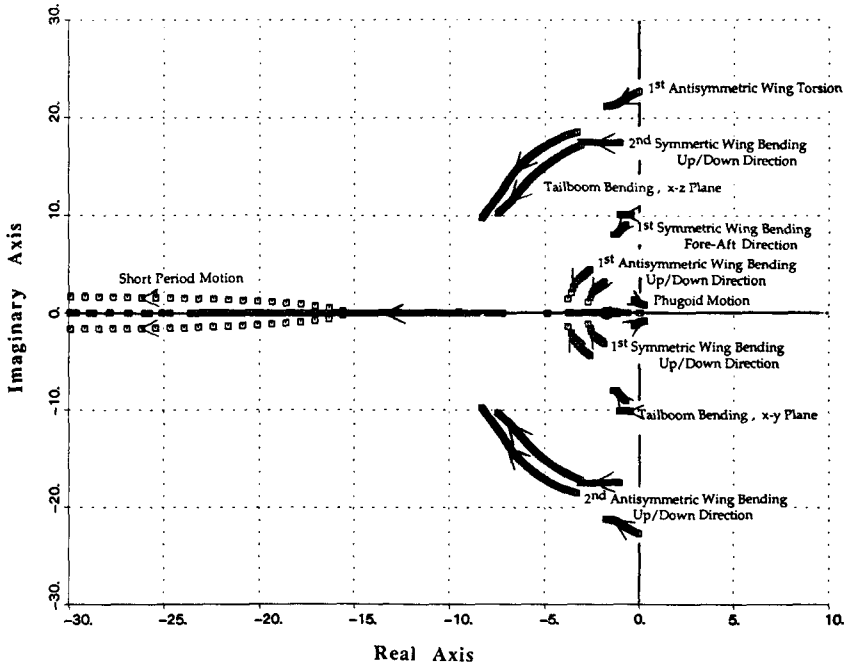

Figure 13 Root locus of the MLE flying at sea level (6-22 m/s). The aeroelastic model includes the first 14 modes (6 rigid and 8 flexible) and unsteady aerodynamics.

Separation of Longitudinal and Lateral Dynamics: Finally Fig. 13 depicts the results obtained with a fourteen degrees of freedom model, six rigid and eight flexible. This model is a complete model of the aircraft and predicts a unstable spiral mode and a stable Dutch roll mode. When these results are compared with the results of Fig.6, one can conclude that the separation of longitudinal and lateral dynamics are justified.

Complex Reduced Frequency: Expression of the Theodorsen function as a complex function of the complex reduced frequency was justified by the relatively high damping ratios predicted by the aeroelastic model. If the reduced frequency was assumed to be real [Hassig], as is normally done in the aeroelastic analyses of lightly damped aircraft, the contribution due to the imaginary (damping) component of the reduced frequency would have been ignored. This would represent a significant mis-modeling of the unsteady aerodynamics.

Summary and Conclusions

This research identified the critical aeroelastic issues that should be considered in the aeroelastic analysis of very flexible, very light aircraft. Given the unverified structural dynamic model, the results can only be seen as preliminary but the trends predicted should yield valuable insight to control and structural engineers. Specifically, the significant motion of the eigenvalues with air speed and altitude indicates that autopilot design will be a critical design activity.

The results indicate that simplification of the aeroelastic model by separation of rigid body modes and flexible modes is not justified and that many flexible modes may be required to yield a reliable aeroelastic model. In terms of modal coupling the inclusion of unsteady aerodynamic drag terms are not required but the damping added to the fore-aft bending modes introduced by these terms may improve the fatigue characteristics of the aircraft.

Future work plans to iteratively refine the finite element model using modal and static tests on the MLE aircraft and also by using a finer finite element mesh. These improvements will significantly increase the confidence in the aeroelastic model and yield an aeroelastic model that can serve as a design basis for the development of high altitude, long endurance aircraft.

References

Bisplinghoff, R.L., Ashley, H., and Halfman, R.L, Aeroelasticity, Addison-Wesley Publishing Company, Inc., Cambridge, MA, February 1955.

Boyd, W.N., "Effect of Chordwise Forces and Deformations due to Steady Lift on Wing Flutter," Ph.D. Thesis, Stanford University, SUDAAR No.508, December 1977.

Cunningham, A.E., "A Collocation Method for Predicting Subsonic Pressure Distribution on Interfering Parallel Wings," 12th ASME Structures, Structural Dynamic and Materials Conference, California, 1971.

Dowell, et al, A Modern Course in Aeroelasticity, Sijthoff and Noordhoff, 1980.

Edwards, J.W., "Unsteady Aerodynamic Modeling and Active Aeroelastic Control," SUDAAR 504, February 1977.

Etkin, B., Dynamics of Flight, John Wiley & Sons, New York, 1959.

Garrick, I.E., "Propulsion of a Flapping and Oscillating Airfoil," NACA Report No. 567, May 1936.

Greenberg, J.M., "Some Considerations on an Airfoil in an Oscillating Stream," NACA-TN 1372, August 1947.

Hall, D.W., Fortenbach, C.D., Dimicelli, B.V., and Parks, R.W., "A Preliminary Study of Solar Powered Aircraft and Associated Power Trains," NASA CR-3699, December 1983.

Hassig, H.J., "An Approximate True Damping Solution of the Flutter Equation by Determinant Iteration," *Journal of Aircraft*, Vol. 8, No. 11, November 1971.

Hill, K.W., "Estimation of Aerodynamic Characteristics from Dynamic Flight Test Data. Dynamic Stability Parameters," AGARD-CP-235, Paper 15, Nov. 1978.

Luke, Y.L. and Dengler, M.A., "Tables of the Theodorsen Circulation Function for Generalized Motion," *Journal of the Aeronautical Sciences*, Vol. 8, No. 7, July 1951.

McCormick, B.W., Aerodynamics, Aeronautics, and Flight Mechanics, John Wiley & Sons, New York, 1979.

Petre, A. and Ashley, H., "Drag Effects on Wing Flutter," *Journal of Aircraft*, Vol. 13, No. 10, October 1976, pp. 755-763.

Press, W.H., Flannery, B.P., TeuKolsky, S.A., and Vetterling, W.T., Numerical Recipes - The Art of Scientific Computing, Cambridge University Press, New York, 1987.

Zerweckh, S.H., Von Flotow, A.H. and Murray, J.E., 1988a, "Flight Testing a Highly Flexible Aircraft; Case Study on the MIT Light Eagle," AIAA Atmospheric Flight Mechanics Conference, Minneapolis, August 1988.

Zerweckh, S.H., Sullivan, R.B., 1988b, "Results of the Flight Test Program with the Light Eagle and the Daedalus Aircraft," NASA Contractor Report, NASA Langley, August 1988.